

CrystEngComm

Accepted Manuscript



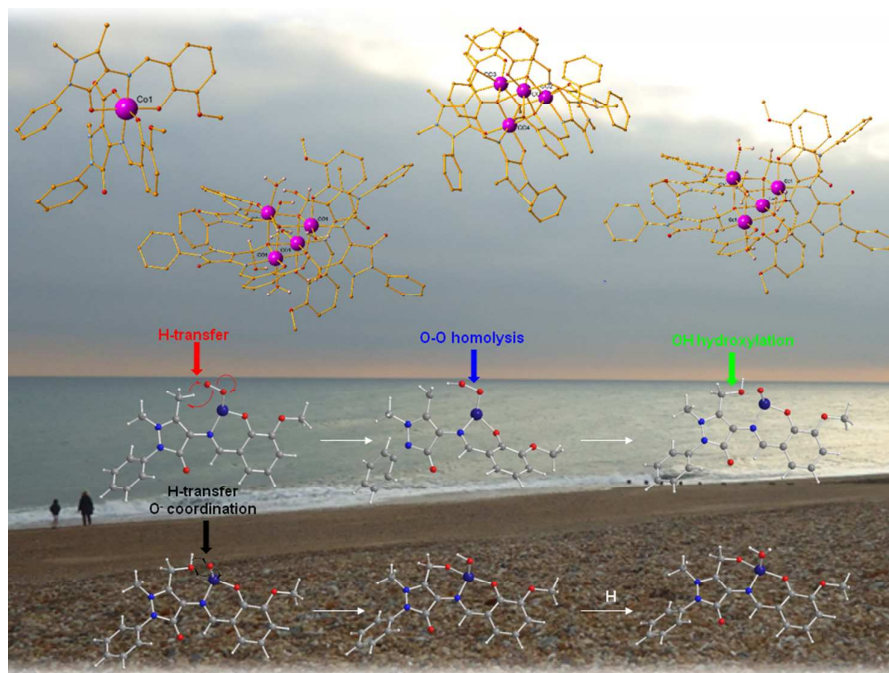
This is an *Accepted Manuscript*, which has been through the Royal Society of Chemistry peer review process and has been accepted for publication.

Accepted Manuscripts are published online shortly after acceptance, before technical editing, formatting and proof reading. Using this free service, authors can make their results available to the community, in citable form, before we publish the edited article. We will replace this *Accepted Manuscript* with the edited and formatted *Advance Article* as soon as it is available.

You can find more information about *Accepted Manuscripts* in the [Information for Authors](#).

Please note that technical editing may introduce minor changes to the text and/or graphics, which may alter content. The journal's standard [Terms & Conditions](#) and the [Ethical guidelines](#) still apply. In no event shall the Royal Society of Chemistry be held responsible for any errors or omissions in this *Accepted Manuscript* or any consequences arising from the use of any information it contains.

Graph Abstract



Nine mono-, di- and tetranuclear coordination clusters ($M = \text{Co}^{\text{II/III}}, \text{Ni}^{\text{II}}, \text{Cu}^{\text{II}}$) using a monoanionic Schiff base ligand were synthesized and characterized by X-ray crystallography. A series of transformations undergo in the ligand in certain compounds, for which theoretical studies are presented. Synthetic aspects, topological issues and magnetic studies are discussed.



Journal Name

ARTICLE

Cobalt(II/III), Nickel(II) and Copper(II) Coordination Clusters employing a monoanionic Schiff base ligand: Synthetic, topological and computational mechanistic aspects

Received 00th January 20xx,
Accepted 00th January 20xx

DOI: 10.1039/x0xx00000x

www.rsc.org/

Edward Loukopoulos,^a Benjamin Berkoff,^a Kieran Griffiths,^a Victoria Keeble,^a Vassiliki N. Dokorou,^a Athanassios C. Tsepis,^{*b} Albert Escuer^c and George E. Kostakis^{*a}

Nine mono-, di- and tetranuclear coordination clusters (M = Co^{II/III}, Ni^{II}, Cu^{II}) using a monoanionic Schiff base ligand were synthesized and characterized by X-ray crystallography. A series of transformations undergo in the ligand in certain compounds, for which theoretical studies are presented. Synthetic aspects, topological issues and magnetic studies are discussed.

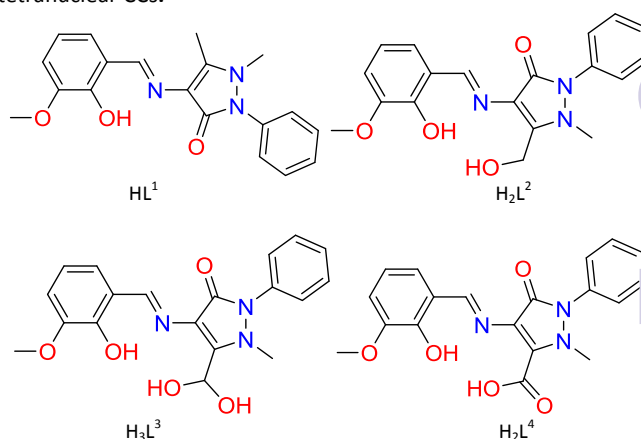
Introduction

Despite its long history and activity, coordination chemistry of polynuclear metal complexes, also known as coordination clusters (CCs),¹ continues to be a field that attracts great interest today. Among the different categories of ligands used in this field, perhaps one of the most significant is Schiff bases, which have received a large amount of attention especially in the last decade. This owes to their wide range of useful properties such as strong biological activity,^{2–4} ease of access and versatile coordination abilities. As a result, CCs using ligands of this nature are of special importance and many examples of their applications in material science,^{5–7} catalysis,^{8–12} biological processes,^{13–15} molecular magnetic materials,^{16–23} photochemistry,^{24,25} and nanostructure studies,^{26,27} have been explored.

In particular, Schiff bases formed from o-vanillin as starting material have been of significant interest and their coordination abilities along with various metal centres have been investigated thoroughly leading to very interesting results.^{28–41} For example, the usage of a Schiff base formed between L-glutamic acid and o-vanillin along with Ni(NO₃)₂·6H₂O results in an intriguing 15-nickel metallomacrocyclic complex.³¹ Ferromagnetic and ferroelectric properties were observed in two enantiomerically pure nanoscale Manganese CCs supported by chiral Schiff base ligands,²⁹ while the pentanuclear compound Mn₃^{III}Ca^{II}Na^I, appeared to be a sufficient

catalyst for water oxidation.⁴²

However, according to a CSD search⁴³ all previous reported o-vanillin-based Schiff base ligands used for the synthesis of polynuclear CCs were derived mainly through a condensation of o-vanillin along with either amino alcohol such as 2-aminoethanol⁴⁴ or amino acid^{31,45} to produce di- or tri-protic organic species. Based on this observation, we recently decided to study the coordination abilities of a Schiff base ligand, derived from the condensation of o-vanillin and 4-aminoantipyrine and named as (E)-4-(2-hydroxy-3-methoxybenzylideneamino)-2,3-dimethyl-1-phenyl-1,2-dihydropyrazol-5-one (HL¹, Scheme 1).⁴⁶ Despite providing similar coordination modes to other diprotic ligands i.e. those derived from o-vanillin and 2-aminoethanol or 2-aminophenol, HL¹ is monoanionic and thus is anticipated to lead to unprecedented topologies. Indeed, the employment of HL¹ in Co^{II}/Dy^{III} chemistry resulted in a series of polynuclear Co^{II}_xDy^{III}_y CCs displaying unseen topologies and interesting magnetic properties.^{46,47} The formation of the aforementioned high nuclearity CC, using solely HL¹, is in contrast to what has been achieved with other diprotic ligands, that provide similar coordination environment, which resulted in tri- or tetranuclear CCs.^{37,48–50}



Scheme 1. The protonated form of (E)-4-(2-hydroxy-3-methoxybenzylideneamino)-2,3-dimethyl-1-phenyl-1,2-dihydropyrazol-5-one (HL¹) ligand used in this study. The different transformations of HL¹ ligand

^a Department of Chemistry, School of Life Sciences, University of Sussex, Brighton BN1 9QJ, UK.

^b Laboratory of Inorganic and General Chemistry, Department of Chemistry, University of Ioannina, 451 10 Ioannina, Greece.

^c Department de Química Inorgànica, Universitat de Barcelona, Diagonal 645, 08028 Barcelona, Spain.

†X-ray crystallographic files in CIF format for structures 1–10. Crystallographic parameters can be found in Tables S1& S2. Scheme S1. Selected bond distances and angles for 1 – 9 can be found in Tables S3-S10. Cartesian coordinates and energies of the Lⁿ (n = 1-4) ligands, the reactant, intermediate, transition state and product cobalt complexes located on the potential energy surfaces of the transformations undergoing the coordinated ligands (Table S12). A library of the 100 polynuclear CCs with nuclearity over 3 is provided as excel file. Electronic Supplementary Information (ESI) available: [details of any supplementary information available should be included here]. See DOI: 10.1039/x0xx00000x

observed in compounds **5–7** (H_2L^2 , H_3L^3 , H_2L^4). Transformed organic molecules are presented in their protonated form.

In this study, we report the initial employment of HL^1 in $\text{Co}^{\text{II,III}}$, Ni^{II} and Cu^{II} chemistry and thus present the synthesis, characterization and crystal structure of nine CCs formulated as $[\text{Co}^{\text{II}}\text{L}^1_2]\cdot 5\text{MeCN}$ (**1**·5MeCN), $[\text{Ni}^{\text{II}}\text{L}^1_2]\cdot 5\text{MeCN}$ (**2**·5MeCN), $[\text{Cu}^{\text{II}}\text{L}^1_2]\cdot \text{MeCN}$ (**3**·MeCN), $[\text{Co}^{\text{II}}\text{L}^1_4(\text{MeO})_2]\cdot 2(\text{ClO}_4)$ (**4**), $[\text{Co}^{\text{II}}\text{L}^2_4(\text{H}_2\text{O})_4]$ (**5**), $[\text{Co}^{\text{II}}\text{L}^3_4(\text{H}_2\text{O})_4]$ (**6**), $[\text{Co}^{\text{II}}\text{L}^1_4]\cdot 2\text{MeCN}$ (**7**·2MeCN), $[\text{Ni}^{\text{II}}_2\text{L}^1_3(\text{MeOH})]\cdot (\text{ClO}_4)_2\cdot 2\text{MeOH}$ (**8**·2MeOH), $[\text{Cu}^{\text{II}}\text{L}^1_4(\text{MeO})_2]\cdot 2(\text{ClO}_4)\cdot 6\text{MeOH}$ (**9**·6MeOH), as well as magnetic properties for representative compounds **4** and **8**. Synthetic and topological issues are discussed. We additionally report interesting cases of ligand transformation found in **4–7**, supported by theoretical density functional theory studies which give valuable insight into the direct mechanism taking place during these transformations.

Experimental

Materials and methods

Materials. Chemicals (reagent grade) were purchased from Sigma Aldrich and Alfa Aesar. All experiments were performed under aerobic conditions using materials and solvents as received. *Safety note:* Perchlorate salts are potentially explosive; such compounds should be used in small quantities and handled with caution and utmost care at all times.

Instrumentation. IR spectra of the samples were recorded over the range of $4000\text{--}650\text{ cm}^{-1}$ on a Perkin Elmer Spectrum One FT-IR spectrometer fitted with a UATR polarization accessory. Elemental analysis data were recorded in Science Centre, London Metropolitan University, 29 Hornsey Road, London N7 7DD.

Magnetic studies. Magnetic susceptibility measurements were carried out on polycrystalline samples with a MPMS5 Quantum Design susceptometer working in the range 30–300 K under external magnetic field of 0.3 T and under a field of 0.03T in the 30 – 2 K range to avoid saturation effects. Diamagnetic corrections were estimated from Pascal Tables.

Computational Details. All calculations were performed using the Gaussian 09 program suite.⁵¹ The geometries of all stationary points located on the potential energy surfaces (PESs) were fully optimized, without symmetry constraints, employing the 1997 hybrid functional of Perdew, Burke, and Ernzerhof^{52–57} as implemented in the Gaussian09 program suite. This functional uses 25% the so-called "exact" exchange, i.e. Hartree-Fock-like exchange built on Kohn-Sham orbitals, E_x^{HF} , 75% of ("pure DFT") GGA exchange in the PBE approximation, E_x^{PBE} , and 100% of GGA correlation in the PBE formulation, E_c^{PBE} and is denoted as PBE0. For the geometry optimizations we have used the Def2-TZVP basis set for Co atoms and the 6-31G(d,p) basis set for all main group elements (E). Hereafter the method used in DFT calculations is abbreviated as PBE0/Def2-TZVP(Co) ∪ 6-31G(d,p)(E). All stationary points were identified as minima (number of imaginary frequencies $\text{Nimag}=0$). Acetonitrile solvent effects were taken into account with the Polarizable Continuum Model (PCM) using the integral equation formalism variant (IEFPCM) being the default self-consistent reaction field (SCRF) method.⁵⁸

Synthetic procedures

Ligand synthesis. The synthesis of HL^1 has been carried out according to the reported synthetic procedure.⁴⁶

Synthesis of $[\text{Co}^{\text{II}}\text{L}^1_2]\cdot 5\text{MeCN}$ (1**·5MeCN).** 0.55 mmol (0.190 g) of HL^1 and 0.55 mmol (77.1 μL) of Et_3N were dissolved in 20 ml MeCN. The resulting yellow solution was brought to reflux and stirred for 10 minutes. To this 0.23 mmol (0.050 g) of CoBr_2 were added and the resulting red solution was refluxed for another 20 minutes, filtered and kept in a vial and subjected to slow evaporation. Red crystals formed within 1 day. Yield: 35% (based on Co). Selected IR peaks (cm^{-1}): 2929 (w), 2820 (w), 1590 (s), 1536 (m), 1492 (m), 1462 (m), 1434 (s), 1389 (s), 1300 (m), 1237 (m), 1209 (s), 1185(s), 1108 (m), 1080 (m), 1045 (m), 972 (m), 921 (w), 878 (w), 853 (w), 786 (w), 740 (s), 702 (s), 678 (m). Analogous reaction with $\text{Co}(\text{ClO}_4)_2\cdot 6\text{H}_2\text{O}$ instead of CoBr_2 at room temperature, affords a powder crystalline material which was found to be isostructural to **1**, by determining the unit cell of the crystals and recording the I.R. spectra.

Synthesis of $[\text{Ni}^{\text{II}}\text{L}^1_2]\cdot 5\text{MeCN}$ (2**·5MeCN).** 0.25 mmol (0.084 g) of HL^1 and 0.25 mmol (34.9 μL) of Et_3N were dissolved in 20 ml MeCN while stirring to produce a yellow solution. To this, 0.1 mmol (0.037 g) of $\text{Ni}(\text{ClO}_4)_2\cdot 6\text{H}_2\text{O}$ were added. The resulting yellow solution was stirred for a further 15 minutes, filtrated, then kept at a stored vial in room temperature. Large green needles were obtained after 2 days. Yield: 55% (based on Ni). Selected IR peaks (cm^{-1}): 2927 (w), 2822 (w), 2247 (w), 1593 (s), 1541 (m), 1496 (m), 1450 (m), 1438 (s), 1393 (m), 1298 (m), 1242 (m), 1208 (s), 1185(s), 1109 (m), 1076 (m), 1047 (m), 974 (s), 922 (w), 878 (w), 847 (w), 820 (w), 781 (w), 741 (s), 702 (s), 686 (m).

Synthesis of $[\text{Cu}^{\text{II}}\text{L}^1_2]\cdot \text{MeCN}$ (3**·MeCN).** 0.25 mmol (0.084 g) of HL^1 and 0.5 mmol (69.0 μL) of Et_3N were dissolved in 20 ml MeCN while stirring to produce a yellow solution. To this, 0.1 mmol (0.020 g) of $\text{Cu}(\text{OAc})_2\cdot \text{H}_2\text{O}$ were added. The resulting dark brown solution was stirred for a further 15 minutes, filtrated, then kept at a stored vial in room temperature. Dark brown block crystals were obtained after 1 day. Yield: 45% (based on Cu). Selected IR peaks (cm^{-1}): 2932 (w), 2830 (w), 1662 (s), 1583 (s), 1538 (m), 1492 (m), 1456 (s), 1434 (m), 1389 (m), 1298 (m), 1242 (m), 1208 (s), 1155 (w), 1109 (m), 1073 (s), 1043 (s), 976 (s), 928 (w), 878 (w), 850 (w), 820 (w), 789 (m), 742 (s), 707 (s), 688 (m). Elemental analysis for $\text{C}_{40}\text{H}_{39}\text{CuN}_7\text{O}_6$: calcd. C 61.81, H 5.06, N 12.61; found C 61.67, H 5.27, N 12.51.

Synthesis of $[\text{Co}^{\text{II}}\text{L}^1_4(\text{MeO})_2]\cdot 2(\text{ClO}_4)$ (4**).** 0.25 mmol (0.084 g) of HL^1 and 0.25 mmol (34.9 μL) of Et_3N were dissolved in 20 ml MeOH while stirring to produce a yellow solution. To this, 0.1 mmol (0.037 g) of $\text{Co}(\text{ClO}_4)_2\cdot 6\text{H}_2\text{O}$ were added. The resulting red solution was stirred for a further 15 minutes, filtrated, then kept at a stored vial in room temperature. Red prismatic crystals were obtained after 5 days. Yield: 25% (based on Co). Selected IR peaks (cm^{-1}): 2935 (w), 2817 (w), 1603 (s), 1583 (s), 1558 (m), 1544 (m), 1489 (w), 1456 (s), 1433 (s), 1391 (m), 1241 (m), 1213 (s), 1194 (m), 1081 (s), 1036 (s), 969 (s), 913 (w), 869 (w), 855 (w), 788 (m), 741 (s), 701 (s), 677 (m).

Synthesis of $[\text{Co}^{\text{II}}\text{L}^2_4(\text{H}_2\text{O})_4]$ (5**).** 0.30 mmol (0.100 g) of HL^1 and 0.30 mmol (41.8 μL) of Et_3N were dissolved in 20 ml MeCN while stirring to produce a yellow solution. To this, 0.24 mmol (0.060 g) of $\text{Co}(\text{OAc})_2\cdot 4\text{H}_2\text{O}$ were added. The resulting red solution was stirred for a further 20 minutes, filtrated, then kept at a stored vial in room temperature. Red block crystals were obtained after 3 days. Yield: 20% (based on Co). Selected IR peaks (cm^{-1}): 2929 (w), 2834 (w), 1623 (s), 1592 (s), 1540 (m), 1497 (m), 1440 (s), 1404 (m), 1311 (m), 1235 (m), 1209 (s), 1072 (s), 1024 (s), 971 (s), 877 (w), 857 (w), 787 (w), 738 (s), 722 (s), 684 (m).

Synthesis of $[\text{Co}^{\text{II}}\text{L}^3_4(\text{H}_2\text{O})_4]$ (6**).** *Method 1:* (**6**) was prepared in the same ratio and solvent as (**3**) by using $\text{Co}(\text{OAc})_2\cdot 4\text{H}_2\text{O}$ and then carefully layering the solution over Et_2O in a respective ratio of 1:2.

Red block crystals were obtained after 1 day. Yield: 35% (based on Co). Selected IR peaks (cm^{-1}): 2935 (w), 2828 (w), 1621 (s), 1592 (s), 1544 (m), 1494 (m), 1445 (s), 1403 (m), 1307 (m), 1239 (m), 1210 (s), 1074 (s), 1026 (s), 967 (s), 875 (w), 856 (w), 811 (w), 737 (s), 719 (s), 690 (m). **Method 2:** 0.56 mmol (0.190g) of L and 1.11 mmol (154.3 μL) of Et_3N were dissolved in 20ml MeCN. The resulting yellow solution was brought to reflux and stirred for 10 minutes. To this 0.46 mmol (0.157 g) of $\text{Co}(\text{BF}_4)_2 \cdot 6\text{H}_2\text{O}$ were added and the resulting red solution was refluxed for another 20 minutes, filtered and kept in a vial and subjected to slow evaporation. Red crystals formed within 1 day. Yield: 20% (based on Co). **Method 3:** 0.56 mmol (0.190g) of L and 2.21 mmol (308.6 μL) of Et_3N were dissolved in 20ml MeCN. The resulting yellow solution was brought to reflux and stirred for 10 minutes. To this 0.45 mmol (0.166 g) of $\text{Co}(\text{ClO}_4)_2 \cdot 6\text{H}_2\text{O}$ were added and the resulting red solution was refluxed for another 20 minutes, filtered and kept in a vial and subjected to slow evaporation. Red crystals formed within 1 day. Yield: 20% (based on Co). Elemental analysis for $\text{C}_7\text{H}_7\text{Co}_4\text{N}_{12}\text{O}_{24}$: calcd. C 51.37, H 4.31, N 9.46; found C 47.67, H 4.15, N 8.74. This result corresponds to the presence of eight water molecules $\text{C}_7\text{H}_7\text{Co}_4\text{N}_{12}\text{O}_{24} (\text{H}_2\text{O})_8$ C 47.49, H 4.82, N 8.75. The crystalline material collected using Methods 2 and 3 was found to be isostructural to that collected using Method 1, by determining the unit cell of the crystals and recording the I.R. spectra.

Synthesis of $[\text{Co}^{\text{II}}\text{L}^1_4] \cdot 2\text{MeCN}$ (7**·2MeCN).** **7** was prepared in the same ratio, metal salt and solvent as (**5**) by refluxing the solution for 20 minutes. The resulting red solution was then filtrated and kept at a stored vial in room temperature. Red block crystals were obtained after 3 days. Yield: 30% (based on Co). Selected IR peaks (cm^{-1}): 2935 (w), 1639 (s), 1621 (s), 1591 (s), 1547 (m), 1492 (m), 1442 (s), 1401 (m), 1302 (m), 1238 (m), 1213 (s), 1077 (s), 1028 (s), 968 (s), 875 (w), 856 (w), 811 (w), 737 (s), 719 (s), 690 (m).

Synthesis of $[\text{Ni}^{\text{II}}\text{L}^1_3(\text{MeOH})] \cdot (\text{ClO}_4)_2 \cdot 2\text{MeOH}$ (8**·2MeOH).** **8** was prepared in the same ratio and solvent as (**4**) by using $\text{Ni}(\text{ClO}_4)_2 \cdot 6\text{H}_2\text{O}$ and then keeping the filtrated solution at a stored vial in room temperature. Large dark yellow crystals were obtained after 2 days. Yield: 35% (based on Ni). Selected IR peaks (cm^{-1}): 2935 (w), 2816 (w), 1603 (s), 1585 (s), 1559 (m), 1543 (m), 1492 (w), 1453 (s), 1436 (s), 1391 (m), 1241 (m), 1213 (s), 1193 (m), 1081 (s), 970 (s), 913 (w), 856 (w), 789 (m), 741 (s), 701 (s), 677 (m). Elemental analysis for $\text{C}_{60}\text{H}_{66}\text{ClN}_9\text{Ni}_2\text{O}_{16}$: calcd. C 54.51, H 5.03, N 9.53; found C 54.33, H 4.88, N 9.41.

Synthesis of $[\text{Cu}^{\text{II}}\text{L}^1_4(\text{MeO})_2] \cdot 2(\text{ClO}_4)_2 \cdot 6\text{MeOH}$ (9**·6MeOH).** 0.1 mmol (0.034 g) of HL^1 and 0.1 mmol (13.9 μL) of Et_3N were dissolved in 20 ml MeOH while stirring to produce a yellow solution. To this, 0.2 mmol (0.074 g) of $\text{Cu}(\text{ClO}_4)_2 \cdot 6\text{H}_2\text{O}$ were added. The resulting dark green solution was stirred for a further 20 minutes, filtrated, then kept at a stored vial in room temperature. Brown block crystals were obtained after 2 days. Yield: 20% (based on Cu). Selected IR peaks (cm^{-1}): 2939 (w), 2817 (w), 1603 (s), 1576 (s), 1558 (m), 1548 (m), 1492 (w), 1451 (s), 1433 (s), 1391 (m), 1241 (m), 1213 (s), 1195 (m), 1081 (s), 974 (s), 916 (w), 869 (w), 855 (w), 791 (m), 742 (s), 701 (s), 677 (m). Elemental analysis for $\text{C}_{84}\text{H}_{102}\text{Cl}_2\text{Cu}_4\text{N}_{12}\text{O}_{28}$: calcd. C 42.15, H 4.01, N 8.19; found C 41.50, H 4.04, N 7.62.

Crystallography

Data for **1**, **2**, **3**, **5**, **6**, **9** and **10** were collected (ω - scans) at the University of Sussex using an Agilent Xcalibur Eos Gemini Ultra diffractometer with CCD plate detector under a flow of nitrogen gas at 173(2) K using Mo $\text{K}\alpha$ radiation ($\lambda = 0.71073 \text{ \AA}$). CRYSLIS CCD and RED software was used respectively for data collection and

processing. Reflection intensities were corrected for absorption by the multi-scan method. Data for **4**, **7** and **8** were collected at the National Crystallography Service, University of Southampton.⁵⁹ All structures were determined using Olex2⁶⁰, solved using either Superflip⁶¹ or SHELXT^{62,63} and refined with SHELXL-2014.⁶⁴ All non-H atoms were refined with anisotropic thermal parameters, and H-atoms were introduced at calculated positions and allowed to ride on their carrier atoms. In compounds **8** and **9** atoms of minor components (several with partial occupancy) were sensibly refined isotropically. Crystal data and structure refinement parameters for all compounds are given in Tables S1 and S2. Geometric/crystallographic calculations were performed using PLATON⁶⁵, Olex2⁶⁰, and WINGX⁶² packages; graphics were prepared with Crystal Maker and MERCURY.⁶⁶ Each of the crystal structures has been deposited at the CCDC 1400124-1400133.

Results and discussion

Crystal Structure Description. Compounds **1** – **3** are monomers synthesized using a 4:5:5, a 2:5:10 or a 2:5:5 metal-ligand-base ratio and acetonitrile as solvent (Figure 1). All compounds crystallize in the triclinic $P\bar{1}$ space group and contain one molecule in the asymmetric unit. Compounds **1** and **2** are isostructural and thus only the former will be further described. Compound **1** is a Co^{II} monomer in which the metal centre has a distorted octahedral geometry, coordinating to two ligand molecules and a total of 6 atoms. Each ligand coordinates to Co^{II} via the phenoxide oxygen atom (O2 and O5 respectively), the imine group nitrogen atom (N1 and N4 respectively) and the carbonyl group oxygen atom (O3 and O6 respectively) (Scheme S1, Mode A). The mean $\text{M}-\text{O}_{\text{phenoxide}}$ distances are 2.0076(19) and 2.0141(16) Å , while the $\text{M}-\text{N}_{\text{imine}}$ were measured at 2.0873(19) and 2.0855(18) Å . $\text{M}-\text{O}_{\text{carbonyl}}$ distances are slightly longer at 2.2458(16) and 2.2286(16) Å , respectively, indicative of a Co^{II} . Similar bond distances for **2** can be found in Supporting Information (Table S3). Five acetonitrile molecules are also present in the crystal lattice. Each molecule is isolated within the crystal structure as there are no hydrogen bonds or other supramolecular interactions formed.

Compound **3** is a Cu^{II} monomer in which the metal centre coordinates to two ligand molecules and a total of 4 atoms, having a distorted square planar geometry. Each ligand coordinates to Cu^{II} via the phenoxide oxygen atom (O2 and O5 respectively) and the imine group nitrogen atom (N1 and N4 respectively) (Scheme S1, Mode B). The mean $\text{M}-\text{O}_{\text{phenoxide}}$ distances are 1.8991(13) Å and 1.9006(14) Å while the $\text{M}-\text{N}_{\text{imine}}$ distances were measured at 1.9671(14) and 1.9532(17) Å , all slightly lower than the respective distances in compounds **1**, **2**. One acetonitrile molecule is also present in the crystal lattice. As in **1** and **2**, no hydrogen bonding or other supramolecular interaction can be found within the crystal structure.

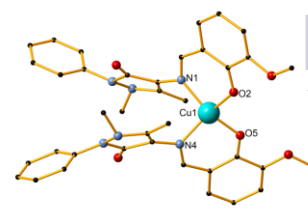
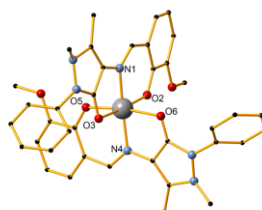


Figure 1. (left) The structure of compounds **1**, **2**. M = Co^{II} (**1**), Ni^{II} (**2**). (right) The structure of compound **3**. H atoms and solvent molecules are omitted for clarity. Colour code M (grey), Cu (light blue), O (red), C (black), N (blue).

Compound **4** is synthesized using a 2:5:5 metal-ligand-base ratio and methanol as solvent and crystallizes in the monoclinic $P2_1/c$ space group. The asymmetric unit contains four metal centres, four ligand molecules, two bridging methoxides and two perchlorate counter ions (Figure 2, upper).

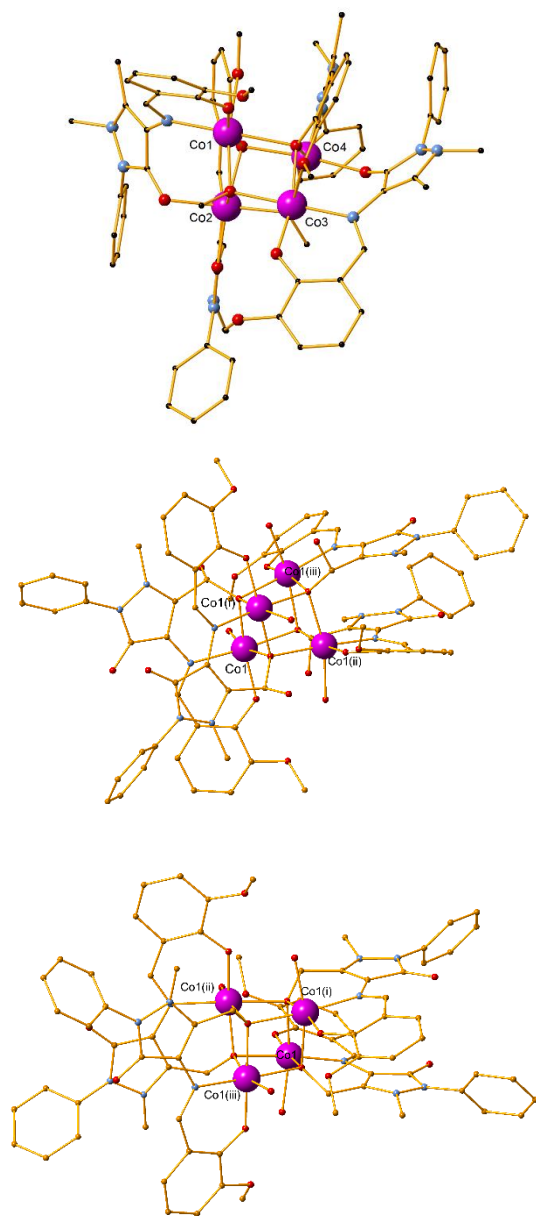


Figure 2. The structure of compounds (upper) **4**, (middle) **5** symmetry operations (i) $1-x, 3/2-y, z$ (ii) $5/4-y, 1/4+x, 1/2-z$ and (iii) $y-1/4, 5/4-x, 1/4-z$, (lower) **6** symmetry operations (i) $1-x, 3/2-y, z$ (ii) $y-1/4, 5/4-x, 5/4-z$ and (iii) $5/4-y, 1/4+x, 5/4-z$. H atoms and lattice molecules are omitted for clarity. Colour code Co (purple), O (red), C (black), N (blue).

The main core of the cluster is a deformed cubane-like Co_4O_4 , consisting of four Co^{II} centres, two bridging μ_3 -O methoxido atoms, and two bridging μ_3 -O phenoxido atoms. Each of the Co^{II} centres coordinates to six atoms and displays a distorted

octahedral geometry. The four organic ligands exhibit two different coordination modes; two ligands per mode. In the first mode, the phenoxide oxygen atom and the imine nitrogen atom coordinate to one Co^{II} centre, while the carbonyl oxygen atom coordinates to a second Co^{II} centre (Scheme S1, Mode C). In the second mode, one Co^{II} centre is coordinated to the phenoxide oxygen atom, the imine nitrogen atom and the carbonyl oxygen atom, while the phenoxide atom is further bridging two Co^{II} centres and the methyl ether group oxygen atom also coordinates to the third Co^{II} centre (Scheme S1, Mode D). The Co^{II}...Co^{II} distances range from 3.018(7) to 3.350(7) Å. Selected bond lengths and angles for **4** are given in Table S10. No hydrogen bonds or other supramolecular interactions can be found between the molecules within the crystal structure.

Compound **5** is synthesized using a 4:5:5 metal-ligand-base ratio and acetonitrile as solvent (Figure 2, middle). As in **4**, a Co_4O_4 cubane-like core is formed, however a transformation of the ligand has taken place; the CH_3 group of the C atom of the pyrazolone ring is oxidized to a CH_2OH , as it was confirmed by X-Ray crystallography (Scheme 1, H_2L^2). Compound **5** has crystallographically imposed bar-4 symmetry and crystallizes in the tetragonal $I4_1/a$ space group and the asymmetric unit consists of one Co^{II} centre, one L^2 ligand and one water molecule. There are no solvent molecules or counter ions present in the structure. The cubane-like Co_4O_4 consists of the four Co^{II} and four bridging μ_3 -O methoxido atoms of the CH_2OH transformed group. Only one type of coordination mode is present in the structure, as the ligand coordinates to the metal center via the imine nitrogen atom (N1), the phenoxide oxygen atom (O2) and the CH_2OH transformed group oxygen atom (O4) (Scheme S1, Mode G). A water molecule also coordinates to each of the cobalt centres, to thus fulfil its distorted octahedral geometry. The mean M-N_{imine} distance was measured at 2.110(2) Å, which is the longest M-N_{imine} bond observed in this study. Co...Co distances range from 3.2064(10) to 3.2157(6) Å. Additional bond distances and angles are given in Table 1. The crystal structure of **5** is stabilized by a strong O-H...O intermolecular hydrogen bond which involves a water oxygen atom (O5) as a donor and the phenoxide oxygen atom (O2) as acceptor. The parameters of this hydrogen bond can be found in Table S4. Compound **6** has crystallographically imposed bar-4 symmetry and is isoskeletal to **4** and **5**. It was synthesized using a 2:5:10 metal-ligand-base ratio and acetonitrile as solvent (Figure 2, right). Reactions with different conditions under a 4:5:10 and a 4:5:20 ratio afforded the same product but in a lower yield. As in **4** and **5**, a Co_4O_4 cubane-like core is formed, however a different transformation of the ligand is observed; the methyl group connected to the pyrazolone ring is, in the present case, transformed to a $CH(OH)_2$ group (Scheme 1, H_3L^3). The two C-O bonds were crystallographically refined, without any restrictions, to 1.346(7) Å and 1.398(4) Å for O4 and O5, respectively, typical to a single C-O bond value. The compound crystallizes in the tetragonal $I4_1/a$ space group and the asymmetric unit consists of one Co^{II} centre, one L^3 ligand and one water molecule. There are no solvent molecules or counter ions present in the structure. The cubane-like Co_4O_4 consists of the four Co^{II} centres and four bridging μ_3 -O atoms; the oxygen atom belongs to the transformed $CH(OH)_2$ group. Only one type of coordination mode is present in the structure, as the ligand coordinates to the metal center via the imine nitrogen atom (N1), the phenoxide oxygen atom (O2) and oxygen atom (O4) (Scheme S1, Mode H).

A water molecule also coordinates to each of the cobalt centres, to fulfil the distorted octahedral geometry. The mean M-N_{imine}

distance was measured at 2.107(3) Å. Co...Co distances range from 3.2207(11) to 3.2277(9) Å. Additional bond distances and angles are given in Table 1. The crystal structure of **6** is stabilized by a strong O-H...O intermolecular hydrogen bond, which involves a water oxygen atom (O6) as a donor and a carbonyl oxygen atom (O3) as acceptor. The structure is further stabilized by a strong O-H...O intramolecular hydrogen bond within two ligands, in which an oxygen atom of the transformed group (O5) participates as a donor. The parameters of these hydrogen bonds are listed in Table S5.

Compound **7** was synthesized using a 4:5:5 metal-ligand-base ratio and acetonitrile as solvent (Figure 3), crystallizes in the triclinic $P\bar{1}$ space group and contains two molecules in the asymmetric unit. Unlike the previous three structures, Bond Valence Sum (BVS) calculations⁶⁷ are indicative of oxidation state III for both Co centers (3.22 for Co1 and 3.24 for Co2). The ligand undergoes another oxidation (H_2L_4 Scheme 1) and the methyl group connected to the pyrazolone ring is transformed to a carboxylate, as assigned by the 1.238(5) Å and 1.275(4) Å bond distances, for C31-O7 and C31-O6, respectively. Each molecule contains a Co^{III} centre, one L¹ and one L⁴ ligand, as well as two acetonitrile solvent molecules. The Co^{III} centre has a distorted octahedral geometry and is coordinated to one L¹ molecule, via the phenoxide oxygen atom, the imine nitrogen atom and the carbonyl group oxygen atom (Scheme 2, Mode A), as well as one L⁴ molecule, via the imine nitrogen atom, the phenoxide oxygen atom and the carboxyl group oxygen atom (Scheme 2, Mode I). The mean M-N_{imine} distances are relatively similar for both ligands (1.929(3) Å for L⁴ coordination, 1.933(3) and 1.937(3) Å for L¹ coordination), while the M-O_{phenoxide} distances are smaller in the case of the L¹ ligand (1.869(3) Å for L¹ coordination, 1.873(3) and 1.885(3) Å for L⁴ coordination). The mean M-O_{carbonyl} distances are 1.970(3) and 1.985(3) Å, significantly larger than the M-O_{carboxyl} distances which were measured at 1.904(3) and 1.912(3) Å. Two acetonitrile molecules are also present in the crystal lattice. As in the previous monomeric compounds (**1-3**), there are no hydrogen bonds or other supramolecular interactions formed between the molecules within the crystal structure.

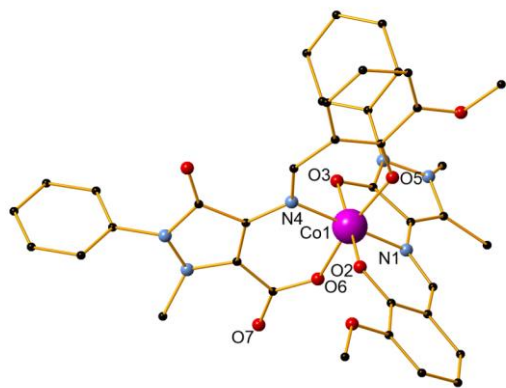


Figure 3. The structure of compound **7**. H atoms and solvent molecules are omitted for clarity. Color code Co (pink), O (red), C (black), N (blue).

Compound **8** is a Ni dimer, synthesized using a 2:5:5 metal-ligand-base ratio and methanol as solvent (Figure 4). It crystallizes in the monoclinic $I2/c$ space group and contains one molecule in the asymmetric unit. Each nickel centre is coordinated to six atoms and displays a distorted octahedral geometry. There are three ligand molecules in the structure and each exhibits a different coordination mode (Scheme 2, Modes A, E, F). Ni1 is coordinated to

two ligands, while Ni2 is coordinated to all three. In detail, Ni1 is coordinated to the carbonyl oxygen atom of one ligand (O6), and the imine nitrogen atoms (N4, N7) as well as the phenoxide oxygen atoms (O5, O8) of two ligand molecules. A terminal methanol solvent molecule also coordinates to the metal centre through the oxygen atom O10. Ni2 is coordinated to phenoxide oxygen atoms from all three ligands (O2, O5, O8), the imine nitrogen atom and phenoxide oxygen atom of one ligand (N1 and O3 respectively), as well as the methyl ether group oxygen atom of a second ligand molecule (O4). Out of the respective Ni-O distances, Ni2-O4 was the longest and was measured at 2.295(3) Å, while Ni1-O5 was the shortest at 1.984(3) Å. Comparing the respective Ni-N distances, the mean Ni1-N4 distance was the longest at 2.085(3) Å, while Ni2-N1 was the shortest at 2.020(3) Å. Selected bond lengths and angles are given in Supporting Information (Table S6). Two perchlorate counter ions are also present in the structure, along with two lattice solvent molecules. The crystal structure of **8** is stabilized by strong O-H...O intermolecular hydrogen bonds, which are formed between either two lattice methanol molecules, or one lattice methanol and a perchlorate anion. Further stabilization occurs with the formation of a strong O-H...O intramolecular hydrogen bond within the ligands. The parameters of these hydrogen bonds are listed in Table S7. Compound **9** is synthesized using a 4 : 2 : 2 metal-ligand-base ratio and methanol as solvent and is isoskeletal⁶⁸ to compound **4** previously described in detail. Bond angles and distances can be found in Supporting Information (Tables S8 and S9)

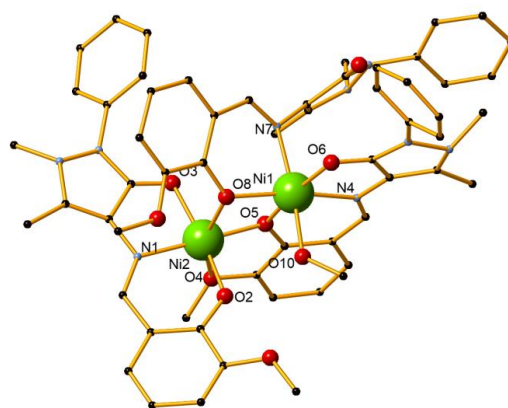
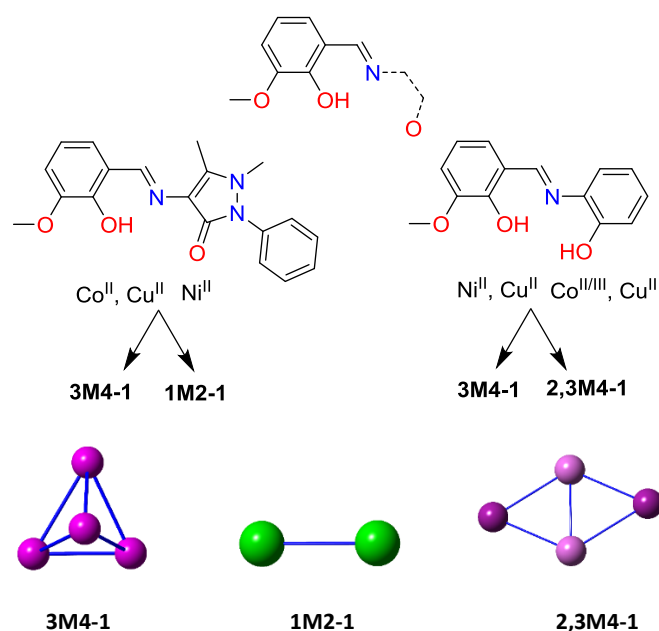


Figure 4. The structure of compound **8**. H atoms and lattice molecules are omitted for clarity. Color code Ni (green), O (red), C (black), N (blue).

Topological features. HL¹ offers similar coordination environment to other diprotic ligands, however in order to identify its unique and different coordination abilities we performed an extended literature CSD search⁴³ seeking on the coordination abilities of any ligand that resembles to Scheme 2, below. Then, we further categorized these findings employing our topological approach to describe CCs,⁶⁹ which resulted in a library of all CCs, with nuclearity over 3 (ESI, excel). The library consists of 100 CCs possessing 29 different motifs. Only 28 entries contain solely 3d (Mn, Fe, Co, Ni and Cu) metal centres. Utilizing HL¹ along with Co^I and Cu^{II}, in methanolic solution, results in cubane Co₄^{II} (**4**) and Cu₄^I (**9**) structures (**3M4-1**, Scheme 2),⁶⁹ in the presence of MeO bridges, and along with Ni(ClO₄)₂·6H₂O in a Ni^{II} dimer (**8**) (**1M2-1**, Scheme 2). In contrast, the reaction of diprotic ligands along with Ni results in a Ni^{II}₄ cubane (**3M4-1**),³⁰ built solely by the organic ligand, while the

Cu forms either a defected dicubane⁷⁰ (**2,3M4-1**, Scheme 2) or a cubane (**3M4-1**) motif.^{44,71} No data were found for Co chemistry, and thus for a structural comparison, we performed the reaction of the diprotic ligand [(E)-2-(2-hydroxy-3-methoxybenzylidene-amino)phenol, H₂L¹] along with Co(ClO₄)₂·6H₂O. The latter reaction resulted in a compound formulated as [Co^{III}₂Co^{II}₂(MeO)₄(L⁵)₂Cl₂] (**10**) (Fig. S4, Table S11) possessing a defect dicubane or **2,3M4-1** topology, indicating sensitivity in oxidation. The transformation of the perchlorate anion to chlorine anion is not unusual and has been seen before.^{72,73} More crystallographic data are necessary to perform a complete structural comparison, however the present findings are indicative that HL¹, despite offering similar coordination sites to other similar diprotic ligands, coordinates completely different to them and thus its coordination chemistry can lead to new, interesting and unprecedented topologies.



Scheme 2 (above) A draw of the organic molecules which resemble similar coordination environment to HL¹ used for the CSD search. (below) A cartoon representation of the Co, Ni, Cu based CCs obtained using different ligands, indicated in the center, and their motif.

Synthetic issues. A detailed analysis of the synthetic aspects for the afforded compounds **1–9** provides very interesting points. There are few parameters that influence the resulting structures. Among these parameters are: a) the solvent which was used, b) the temperature in which the syntheses took place and c) the metal source used. From the resulting compounds it becomes evident that these attributes affect the metal nuclearity and the coordination modes of the ligand to the metal centres, but also facilitate the ligand transformations which were observed in compounds **4–7**.

In regards to the solvent which was used, the afforded compounds can be divided into two categories: a) those which were obtained using a polar solvent such as methanol (compounds **4, 8, 9**) and b) those which were obtained using a non-polar solvent i.e. acetonitrile (compounds **1-3, 5-7**). An immediate observation is the change in the metal nuclearity which also seems to be connected to the ligand transformations; the reaction in protic solvent affords compounds **4, 8** and **9** which are either dimers or tetramers (Co₄, Ni₂, Cu₄), however upon using acetonitrile the respective

monomeric Co (**1**), Ni (**2**), and Cu (**3**) compounds are obtained. In addition, the room temperature reaction of Co(ClO₄)₂·6H₂O with HL¹ in MeCN, results, in low yield, in a powder crystalline material which was found to be the mononuclear compound **1**, however a similar reaction in MeOH results in the formation of the tetranuclear Co^{II} **4**.

It is well known that Co based catalysts have been used in the oxidation of alkanes for the synthesis of terephthalic acid or for adipic acid's synthesis, involving molecular O₂.⁷⁴ In Table 2, a synthetic overview of the synthesis of compounds **1, 4, 5, 6** and **7** is given, where transformation of the organic ligand is observed. In regards of the temperature in which the syntheses of the aforementioned compounds took place two major conclusions can be drawn. a) The room temperature reaction of HL¹, Co(ClO₄)₂·6H₂O in MeCN afforded compound **1** (entry 2), however when a similar reaction is performed under reflux, then a ligand transformation occurs (H₃L³, Scheme 1) affording compound **6** (entry 7). b) A comparison of the synthetic protocol of compounds **5** and **7**, indicates that these two molecules derived using the same metal salt Co(OAc)₂·4H₂O, solvent (MeCN) and metal-ligand-base ratio (4 : 5 : 5); however, room temperature conditions favor the formation of a cobalt tetramer with the transformed L² ligand found in **5** (entry 4), while reflux conditions lead towards the synthesis of a cobalt monomer with a mix of L¹ and L⁴ ligands, found in **7** (entries 4 & 8, respectively).

From this table, another two important notes can be pointed out, both related with the synthesis of compound **6**. First, repeating the room temperature reaction that affords **5** and layering the resultant solution with Et₂O, compound **6** is afforded (entry 5). Second, the latter compound can be obtained from the reaction of HL¹ with Co(BF₄)₂·6H₂O in MeCN under reflux conditions (entry 6). In regards of the organic ligand's transformations found in **5, 6** and **7** (entries 4–8), these are dependent on i) the temperature (entries 4 & 8), ii) the Co source used (entries 6–8) and iii) the presence of Et₂O (entry 5).

Table 2. Synthetic overview for compounds **1, 4–7**.

Entries	Metal Salt	T	Solvent	Ratio (M:L:B)	Compound	Ligand
1	CoBr ₂	Reflux	MeCN	4:5:5	1	L ¹
2	Co(ClO ₄) ₂ ·6H ₂ O	r.t	MeCN	4:5:5	1	L ¹
3	Co(ClO ₄) ₂ ·6H ₂ O	r.t	MeOH	2:5:5	4	L ¹
4	Co(OAc) ₂ ·4H ₂ O	r.t	MeCN	4:5:5	5	L ²
5	Co(OAc) ₂ ·4H ₂ O	r.t	MeCN, Et ₂ O	2:5:10	6	L ³
6	Co(BF ₄) ₂ ·6H ₂ O	Reflux	MeCN	4:5:10	6	L ³
7	Co(ClO ₄) ₂ ·6H ₂ O	Reflux	MeCN	4:5:20	6	L ³
8	Co(OAc) ₂ ·4H ₂ O	Reflux	MeCN	4:5:5	7	L ¹ , L ⁴

Computational mechanistic studies. A comprehensive and consistent picture of the transformations undergoing the coordinated ligands to Co complexes under study (cf. Scheme 1) has been derived by means of DFT calculations employing the PBE0/Def2-TZVP(Co) ∪ 6-31G(d,p)(E) (E = main group element) computational protocol. All crucial reaction steps have been

scrutinized by examining, in terms of located structures, energies and activation barriers, the participation of Co-O₂ intermediates. First we calculated the equilibrium geometries and the electronic structure of the “free” ligands Lⁿ (n = 1-4) in MeCN solutions. Figure 5 shows the ground state geometries of the “free” ligands Lⁿ, the natural atomic charges on selected atoms and the frontier molecular orbitals relevant to coordination of the ligands in MeCN solutions calculated by the PBE0/6-31G(d,p)/PCM computational protocol.

Perusal of the highest occupied molecular orbitals (HOMOs) of the “free” Lⁿ ligands reveals that the electron density is primarily localized on the phenoxide moieties including also the localization on the 2p AOs of the O and N donor atoms of the ligands. These atoms acquire negative natural atomic charges, namely -0.667 - -0.722 |e| on the phenoxide O atom, -0.592 - -0.677 |e| on the carbonyl group O atom, -0.526 - -0.531|e| on the methoxide O atom and -0.514 - -0.576|e| on the imine group nitrogen atom. Both the nature of the HOMOs and the negative natural atomic charges show that all these atoms could participate in the coordination of the Lⁿ ligands to Co central atom, thus explaining all coordination modes observed experimentally (Scheme S1).

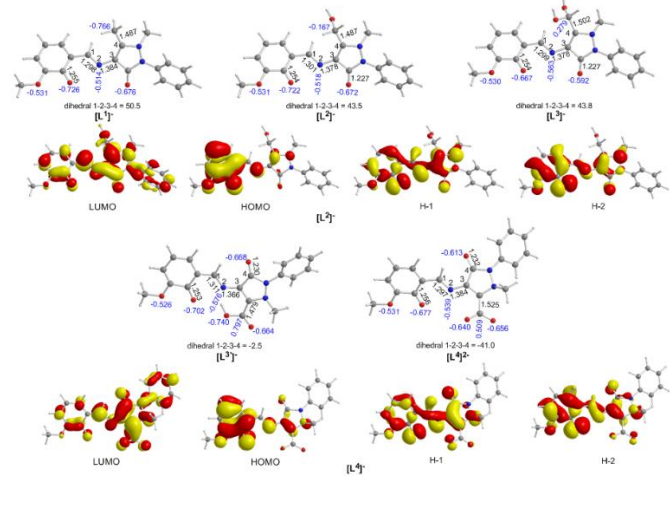
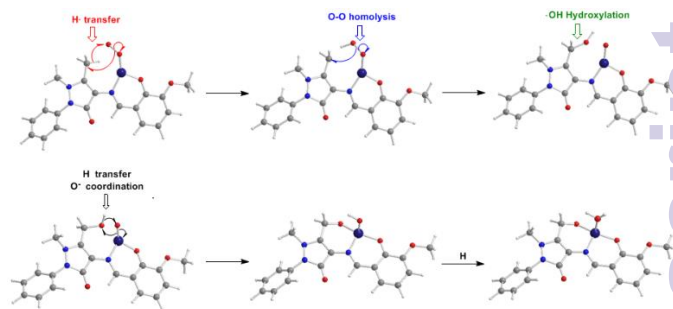


Figure 5. Equilibrium geometries of the “free” ligands Lⁿ, the natural atomic charges on selected atoms (in blue) and the frontier molecular orbitals relevant to coordination of the ligands in MeCN solutions calculated by the PBE0/6-31G(d,p)/PCM computational protocol.

To probe the “distant” intramolecular C-H bond activation by the coordinated superoxide ligand of the C-H bonds of the -CH₃, -CH₂OH and -CH(OH)₂ substituents on the C atom of the pyrazolone ring of the ligands Lⁿ, that promotes the L¹ → L² → L³ → L^{3'} → L⁴ ligand transformations, the reaction trajectory was explored through DFT calculations of the potential energy surfaces (PESs) and monitoring the geometric and energetic reaction profiles (Figures 6-8). A possible reaction mechanism is shown in Scheme 3.



Scheme 3. Proposed mechanism for the intramolecular ligand transformations induced by the [LⁿCo^{II}]⁺ model complexes.

In a first step, the [LⁿCo^{II}]⁺ complexes interact with dioxygen forming the superoxo [LⁿCo(O-O)]⁺ adducts. The formation of the superoxo [LⁿCo(O-O)]⁺ adducts correspond to exothermic processes, the estimated exothermicities are around -18.1 - -18.5 kcal/mol at the PBE0/Def2-TZVP(Co) ∪ 6-31G(d,p)(E)/PCM level of theory. In the superoxo [LⁿCo(O-O)]⁺ complexes the spin density, which was localized at the metal center in the precursor [LⁿCo^{II}]⁺ complexes, is now localized on the superoxide ligand (Scheme 4).

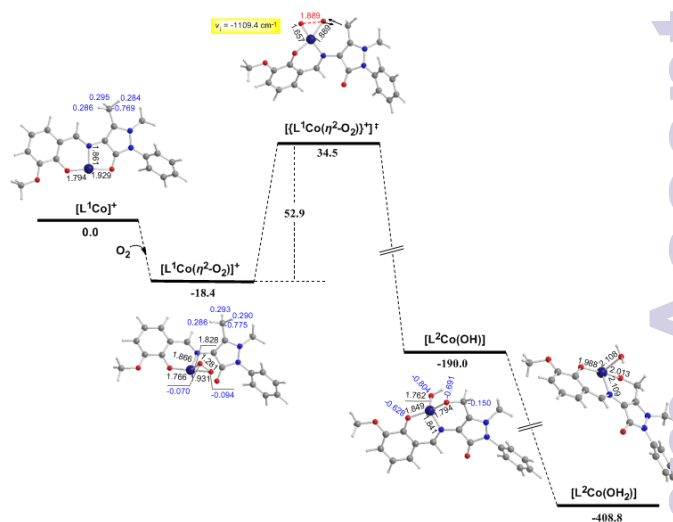
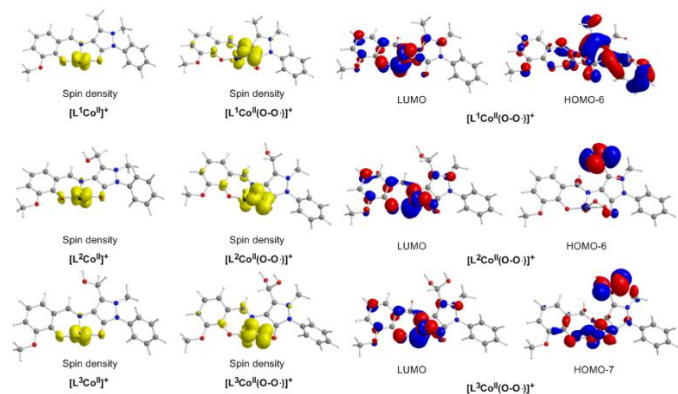


Figure 6. Geometric and energy profile of the reaction trajectory for the intramolecular transformation of coordinated ligand L¹ to L² calculated by the PBE0/Def2-TZVP(Co) ∪ 6-31G(d,p)(E)/PCM (E = main group element, computational protocol).

An inspection of Figures 6-8 reveals that the [LⁿCo]⁺ (n = 1-3) complexes of Co^{II} in their doublet ground states bind O₂ in an asymmetric side-on η²-O₂ coordination mode with a O-O bond length of 1.28 Å, intermediate between the values of 1.21 Å for O₂ and 1.34 Å for O₂²⁻. This bonding mode involving a one electron transfer from the Co^{II} metal center to the dioxygen ligand gives rise to the formation of superoxo [LⁿCo(O-O)]⁺ complexes. In the superoxo [LⁿCo(O-O)]⁺ complexes the Co-O bond lengths for the shorter Co-O bonds are 1.866, 1.839, 1.827 and 1.822 Å for the L¹Co(O-O)]⁺, L²Co(O-O)]⁺, L³Co(O-O)]⁺ and L^{3'}Co(O-O)]⁺ complexes respectively and for the longer Co-O bonds are 1.931, 1.914, 1.930 and 1.937 Å, respectively.



Scheme 4. 3-D plots of the spin density distribution (isospin surfaces = 0.002) in the $[L^nCo]^+$ and $[L^nCo(O-O)]^+$ ($n = 1-3$) model complexes along with the 3-D plots of the molecular orbitals of the $[L^nCo(O-O)]^+$ complexes which support the hydrogen transfer.

It is worth to be noticed that in 1:1 metal- O_2 complexes both the end-on (η^1 -) and side-on (η^2 -) bonding modes have been identified so far and the corresponding adducts were defined as superoxo or peroxy complexes respectively based primarily on the X-ray structural data (O-O bond distance) and vibrational spectra (O-O stretching frequency, ν_{O-O}).⁷⁵⁻⁷⁹

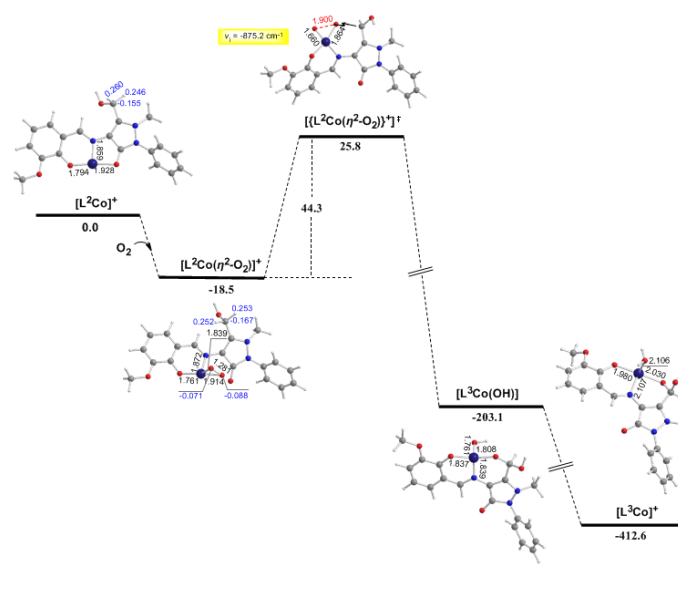


Figure 7. Geometric and energy profile of the reaction trajectory for the intramolecular transformation of coordinated ligand L^2 to L^3 calculated by the PBE0/Def2-TZVP(Co) \cup 6-31G(d,p)(E)/PCM (E = main group element) computational protocol.

In particular, when the O-O bond length is $\approx 1.4 - 1.5 \text{ \AA}$ and the $\nu_{O-O} \approx 800 - 930 \text{ cm}^{-1}$ the compounds are designated as peroxides, whereas when $O-O \approx 1.2-1.3 \text{ \AA}$ and $\nu_{O-O} \approx 1050-1200 \text{ cm}^{-1}$ the compounds are characterized as superoxides. In the model $[L^nCo(O-O)]^+$ complexes the O-O bond length of 1.28 \AA and the unscaled ν_{O-O} stretching vibrational frequencies around $1299-1317 \text{ cm}^{-1}$ illustrate their superoxo character. Although for the superoxide ligand the more common coordination is the end-on coordination (η^1-O_2) it is also well be coordinated in the side-on fashion (η^2-O_2)^{80,81}, as it is the case of the model $[L^nCo(O-O)]^+$ complexes. The

calculated Co-N_{imine} distances in the $[L^nCo]^+$ and $[L^nCo(O_2)]^+$ model complexes are found in the range of $1.859 - 1.867 \text{ \AA}$ and $1.849 - 1.872 \text{ \AA}$ respectively, while the Co-O_{phenoxide} distances are found in the range of $1.918 - 1.929 \text{ \AA}$ and $1.917 - 1.937 \text{ \AA}$ respectively.

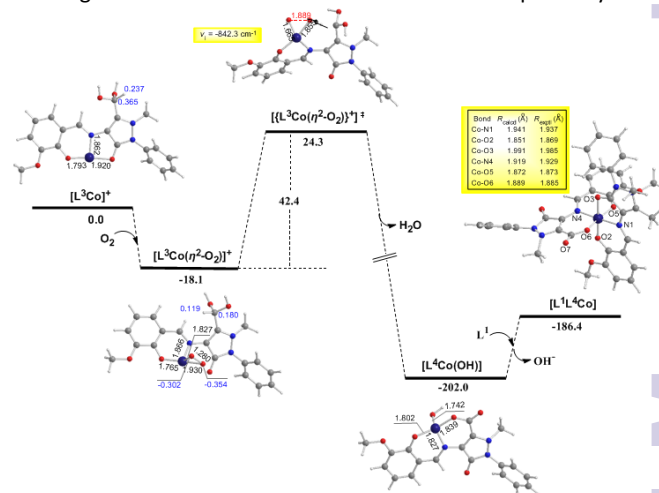


Figure 8. Geometric and energy profile of the reaction trajectory for the intramolecular transformation of coordinated ligand L^3 to L^4 calculated by the PBE0/Def2-TZVP(Co) \cup 6-31G(d,p)(E)/PCM (E = main group element) computational protocol.

The coordinated superoxo radical abstracts a hydrogen atom through a homolytic C-H bond cleavage (*H*-transfer) supported by both electrostatic and orbital interactions. An intramolecular electrophilic attack of the C atom of the $-CH_3$ and $-CH_2OH$ groups by the negatively charged coordinated superoxo radicals is precluded due to the negative natural atomic charges bearing the C atoms of these groups (-0.775 and $-0.167 |e|$ respectively). The orbital interactions supporting the hydrogen transfer in the $[L^nCo(O-O)]^+$ complexes correspond predominantly to HOMO-6 \leftrightarrow LUMO and HOMO-7 \leftrightarrow LUMO interactions (Scheme 4). After the hydrogen abstraction of C-H bond a homolytic O-O bond cleavage (*O-O homolysis*) in the $Co^{II}-OOH$ species takes place affording $Co^{III}=O$ ($\leftrightarrow Co^{II}-O\cdot$) and $HO\cdot$ radical which attacks the C atoms of the CH_3 , CH_2OH and $CH(OH)_2$ groups in nearly concerted fashion (*·OH hydroxylation*) yielding the hydroxylated ligands L^2 , L^3 and L^3 predominantly (Figures 6-8). Furthermore, the active $Co^{III}=O$ ($\leftrightarrow Co^{II}-O\cdot$) species generated after the homolytic O-O bond cleavage could perform cooperatively a second C-H bond cleavage step (*H*-transfer) yielding the $[L^nCo(OH)]$ ($n = 2-4$) intermediates, which subsequently are transformed to the $[L^2Co(OH_2)]$, $[L^3Co(OH_2)]$ and $[L^4Co]$ products. These transformations are predicted to be highly exothermic, the estimated exothermicities are -190.0 , -203.1 and -202.0 kcal/mol for the $L^1 \rightarrow L^2$, $L^2 \rightarrow L^3$ and $L^3 \rightarrow L^4$ ligand transformations respectively. The superoxo $[L^nCo(O-O)]^+$ complexes are transformed to $[L^nCo(OH)]$ ($n = 2-4$) intermediates through the $[[L^nCo(O_2)]^+]^\ddagger$ transition states surmounting an activation barrier of 52.9 , 44.3 and 42.4 kcal/mol for the $L^1 \rightarrow L^2$, $L^2 \rightarrow L^3$ and $L^3 \rightarrow L^4$ ligand transformations respectively. The lowering of the activation barrier along the $L^1 \rightarrow L^2$, $L^2 \rightarrow L^3$ and $L^3 \rightarrow L^4$ ligand transformations could be attributed to the increase of the electrophilic character of the C atom of the $-CH_3$, $-CH_2OH$ and $-CH(OH)_2$ groups, which facilitates the *·OH hydroxylation* process. An analogous reaction trajectory was proposed by Wada and co-workers⁸² for the stoichiometric oxidations of substrates by the non-heme mononuclear hydroperoxo- Fe^{III} complex and more

recently by Li *et al.*⁸³ in the proposed mechanism of dioxygen-activating non-heme enzymes.

Magnetic studies. The room temperature χT value for compound **4** under an applied field of 3000 G is $8.64 \text{ cm}^3 \text{K mol}^{-1}$ which is higher than that of the spin only value of $7.48 \text{ cm}^3 \text{K mol}^{-1}$ for four Co^{II} (Co^{II} ; $S=3/2$ and $g=2.0$). The χT value gradually decreases with decreasing temperature reaching a plateau around 10-20 K and then sharply falls down to $5.17 \text{ cm}^3 \text{K mol}^{-1}$ at 1.8 K. (Figure 9). The non-continuous χT decay evidences some coupling inside the cube in addition to the usual D_{ion} . To have a roughly approach to the $\text{Co}^{\text{II}} \cdots \text{Co}^{\text{II}}$ interactions fit of the experimental data was performed with PHI program⁸⁴ assuming a distorted cube of four $S = 3/2$ spins on basis on the Hamiltonian: $H = -J_1(S_1 \cdot S_4 + S_2 \cdot S_3) - J_2(S_1 \cdot S_2 + S_1 \cdot S_3) - J_3(S_2 \cdot S_3 + S_2 \cdot S_4)$ which corresponds to a cube with similar interactions in opposite faces. Taking into account a D_{ion} term, an excellent fit was obtained for the parameters $J_1 = +4.4 \text{ cm}^{-1}$, $J_2 = +1.3 \text{ cm}^{-1}$, $J_3 = -1.4 \text{ cm}^{-1}$, $g = 2.12$ and $D_{\text{ion}} = 18.8 \text{ cm}^{-1}$. The positive J_1 interaction can be assigned to the pair of faces with lower Co-O-Co bond angles, close to 94-95°. Magnetization experiments performed at 2 K, show a constant increase of magnetization up to a quasi saturated value equivalent to 5.91 electrons under the maximum external field of 5 T, (Figure 9, inset). Each Co^{II} can be treated as an effective $S = 1/2$ spin at low temperature due to the ZFS and thus the magnetization must behaves as an strongly anisotropic effective $S = 2$ spin level. Fit of the magnetization assuming the above response gives an excellent agreement for $D_{S=2} = -1.7 \text{ cm}^{-1}$ and $g = 3.10$.

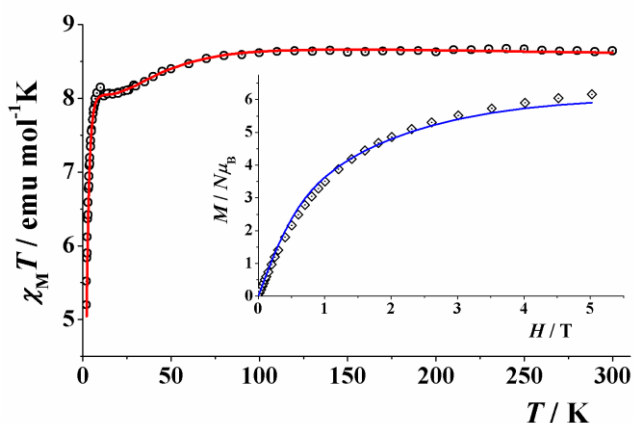


Figure 9. Product of χ_M vs. T for compound **4**. (Inset) magnetization plot in the range 0-5 T. Solid lines show the best obtained fits.

The room temperature $\chi_M T$ value for compound **8** is $2.57 \text{ cm}^3 \text{K mol}^{-1}$ which is higher than that of the spin only value of $2.33 \text{ cm}^3 \text{K mol}^{-1}$ for two Ni^{II} , Figure 10. Upon cooling, this value starts to increase to a maximum value of $2.62 \text{ cm}^3 \text{K mol}^{-1}$ at 20 K and then decreases to $1.68 \text{ cm}^3 \text{K mol}^{-1}$ at 2 K. Magnetization measurements show a continuous increase of magnetization up to a maximum value equivalent to 3.2 electrons. This behavior suggest weak ferromagnetic coupling with $S = 2$ ground state and a significant D contribution. Simultaneous fit of the experimental data was performed applying the Hamiltonian $H = -J(S_1 \cdot S_2)$ and including a D_{ion} parameter. The Least-squares fitting of the experimental data gave the common values for both measurements of $J = +1.2 \text{ cm}^{-1}$, $g = 2.255$, $D = 3.79 \text{ cm}^{-1}$. The fit confirms a $S = 2$ ground state for **8**.

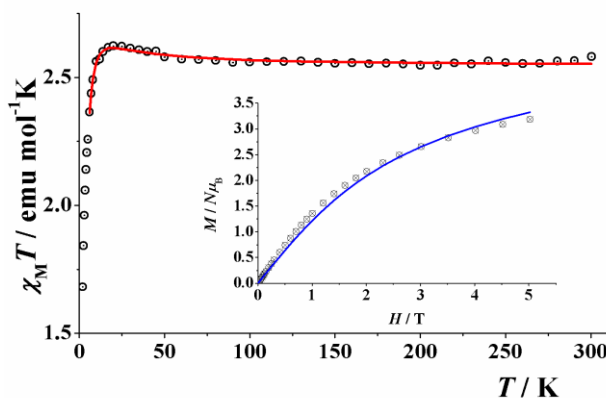


Figure 10. Product of χ_M vs. T for compound **8**. (Inset) magnetization plot in the range 0-5 T. Solid lines show the best obtained simultaneous fit.

Conclusions

In this work we have successfully, for the first time, employed the monoanionic Schiff base ligand (HL^1 , Scheme 1) derived from the condensation of o-vanillin and 4-aminoantipyrine, in Cobalt, Nickel and Copper chemistry to access nine new CCs. A topological evaluation of all polynuclear CCs obtained is reported. In addition, a structural comparison of the present polynuclear CCs along with compounds derived from structural related ligands is attempted (Scheme 2), concluding that: a) HL^1 coordinates completely different to them and thus its coordination chemistry can lead to new, interesting and unprecedented topologies and b) more synthetic studies are required to reach to a point that the design of such species can be undertaken.⁸⁵ We additionally report interesting cases of ligand transformation (Scheme 1), which take place in certain experiments with cobalt sources (**4** – **7**). These transformations occur in one of the methyl groups of the pyrazolone ring of the HL ligand under specific conditions such as the use of particular metal salt, ratio and solvent, altering drastically the coordination mode of the ligand and resulting in different structures. DFT calculations of the potential energy surfaces (PESs) and monitoring the geometric and energetic reaction profiles of the intramolecular $\text{L}^1 \rightarrow \text{L}^2 \rightarrow \text{L}^3 \rightarrow \text{L}^3' \rightarrow \text{L}^4$ ligand transformations, revealed a possible reaction mechanism that involves formation of superoxo $[\text{L}^n \text{Co}(\text{O}-\text{O})]^\dagger$ adducts, which are transformed to $[\text{L}^n \text{Co}(\text{OH})]$ ($n = 2-4$) intermediates through the $\{[\text{L}^n \text{Co}(\text{O}_2)]^\ddagger\}^\ddagger$ transition states surmounting an activation barrier of 52.9, 44.3 and 42.4 kcal/mol for the $\text{L}^1 \rightarrow \text{L}^2$, $\text{L}^2 \rightarrow \text{L}^3$ and $\text{L}^3 \rightarrow \text{L}^4$ ligand transformations respectively. These transformations involve concomitant H -transfer, $\text{O}-\text{O}$ -homolysis and $\cdot\text{OH}$ -hydroxylation processes afford the $[\text{L}^n \text{Co}(\text{OH})]$ ($n = 2-4$) intermediates that subsequently are transformed to the final products. The present findings indicate that coordination chemistry of HL^1 can lead to unprecedented CCs bearing interesting properties and thus our future studies will be focused to further explore it.

Acknowledgements

We thank the EPSRC UK National Crystallography Service at the University of Southampton for the collection of the crystallographic data for compounds **4**, **7** and **8**. Research Development Funding from the University of Sussex is grateful

acknowledged (V. N. D.). V. K. acknowledges University of Sussex for a Junior Research Award summer fellowship. Support from CICYT Project CTQ2012-30662 is acknowledged (A. E.)

Notes and references

- L. Cronin and J. Fielden, in *Coordination Clusters in Encyclopedia of Supramolecular Chemistry*, Taylor and Francis, London, 2007, Taylor & Francis, 2007, pp. 1–10.
- E. Ritter, P. Przybylski, B. Brzezinski, and F. Bartl, *Curr. Org. Chem.*, 2009, **13**, 241–249.
- M. S. Karthikeyan, D. J. Prasad, B. Poojary, K. Subrahmanya Bhat, B. S. Holla, and N. S. Kumari, *Bioorganic Med. Chem.*, 2006, **14**, 7482–7489.
- M. J. O'Donnell, *Acc. Chem. Res.*, 2004, **37**, 506–517.
- R. J. P. Corriu, E. Lancelle-Beltran, A. Mehdi, C. Rey , S. Brand s, and R. Guilard, *J. Mater. Chem.*, 2002, **12**, 1355–1362.
- R. J. P. Corriu, E. Lancelle-Beltran, A. Mehdi, C. Rey , S. Brand s, and R. Guilard, *Chem. Mater.*, 2003, **15**, 3152–3160.
- F. Faridbod, M. R. Ganjali, R. Dinarvand, P. Norouzi, and S. Riahi, *Sensors*, 2008, **8**, 1645–1703.
- K. C. Gupta and A. K. Sutar, *Coord. Chem. Rev.*, 2008, **252**, 1420–1450.
- P. G. Cozzi, *Chem. Soc. Rev.*, 2004, **33**, 410–421.
- D. Ramakrishna, B. R. Bhat, and R. Karvembu, *Catal. Commun.*, 2010, **11**, 498–501.
- Z. Ma, L. Wei, E. C. B. A. Alegria, L. M. D. R. S. Martins, M. F. C. Guedes da Silva, and A. J. L. Pombeiro, *Dalton Trans.*, 2014, **43**, 4048–4058.
- D. S. Nesterov, E. N. Chygorin, V. N. Kokozay, V. V. Bon, R. Bo a, Y. N. Kozlov, L. S. Shul'pina, J. Jezierska, A. Ozarowski, A. J. L. Pombeiro, and G. B. Shul'pin, *Inorg. Chem.*, 2012, **51**, 9110–9122.
- C. M. Da Silva, D. L. Da Silva, L. V. Modolo, R. B. Alves, M. A. De Resende, C. V. B. Martins, and  . De F tima, *J. Adv. Res.*, 2011, **2**, 1–8.
- P. Vicini, A. Geronikaki, M. Incerti, B. Busonera, G. Poni, C. A. Cabras, and P. La Colla, *Bioorganic Med. Chem.*, 2003, **11**, 4785–4789.
- W. Chen, Y. Li, Y. Cui, X. Zhang, H. L. Zhu, and Q. Zeng, *Eur. J. Med. Chem.*, 2010, **45**, 4473–4478.
- H. Miyasaka, R. Cl rac, W. Wernsdorfer, L. Lecren, C. Bonhomme, K.-I. Sugiura, and M. Yamashita, *Angew. Chem. Int. Ed.*, 2004, **43**, 2801–2805.
- S. Mandal, G. Rosair, J. Ribas, and D. Bandyopadhyay, *Inorg. Chim. Acta*, 2009, **362**, 2200–2204.
- Z. L , M. Yuan, F. Pan, S. Gao, D. Zhang, and D. Zhu, *Inorg. Chem.*, 2006, **45**, 3538–48.
- N. C. Anastasiadis, D. A. Kalofolias, A. Philippidis, S. Tzani, C. Raptopoulou, V. Psycharis, C. J. Milios, A. Escuer, and S. P. Perlepes, *Dalton Trans.*, 2015, **44**, 10200–10209.
- A. A. Athanasopoulou, M. Pilkington, C. P. Raptopoulou, A. Escuer, and T. C. Stamatatos, *Chem. Commun.*, 2014, **50**, 14942–14945.
- D. I. Alexandropoulos, T. N. Nguyen, L. Cunha-Silva, T. F. Zafiroopoulos, A. Escuer, G. Christou, and T. C. Stamatatos, *Inorg. Chem.*, 2013, **52**, 1179–1181.
- A. B. Canaj, D. I. Tzimopoulos, A. Philippidis, G. E. Kostakis, and C. J. Milios, *Inorg. Chem.*, 2012, **51**, 10461–10470.
- A. B. Canaj, D. I. Tzimopoulos, A. Philippidis, G. E. Kostakis, and C. J. Milios, *Inorg. Chem. Commun.*, 2012, **51**, 7451–7453.
- K.-H. Chang, C.-C. Huang, Y.-H. Liu, Y.-H. Hu, P.-T. Chou, and Y.-C. Lin, *Dalton Trans.*, 2004, 1731–1738.
- H.-C. Lin, C.-C. Huang, C.-H. Shi, Y.-H. Liao, C.-C. Chen, Y.-C. Lin, and Y.-H. Liu, *Dalton Trans.*, 2007, 781–791.
- L. A. Saghatforoush, R. Mehdizadeh, and F. Chalabian, *Transit. Met. Chem.*, 2010, **35**, 903–910.
- B. Tamami and S. Ghasemi, *Appl. Catal. A Gen.*, 2011, **393**, 242–250.
- E. C. Constable, C. E. Housecroft, J. A. Zampese, and G. Zhan, *Polyhedron*, 2012, **44**, 150–155.
- C.-M. Liu, R.-G. Xiong, D.-Q. Zhang, and D.-B. Zhu, *J. Am. Chem. Soc.*, 2010, **132**, 4044–4045.
- S. Saha, S. Pal, C. J. G mez-Garc a, J. M. Clemente-Juan, K. Harms, and H. P. Nayek, *Polyhedron*, 2014, **74**, 1–5.
- Y. Thio, S. W. Toh, F. Xue, and J. J. Vittal, *Dalton Trans.*, 2014, **43**, 5998–6001.
- H. Oshio, N. Hoshino, T. Ito, M. Nakano, F. Renz, and P. G tlich, *Angew. Chem. Int. Ed.*, 2003, **42**, 223–225.
- N. Hoshino, A. M. Ako, A. K. Powell, and H. Oshio, *Inorg. Chem.*, 2009, **48**, 3396–407.
- M. Sarwar, A. M. Madalan, C. Tiseanu, G. Novitchi, C. Maxim, C. Marinescu, D. Luneau, and M. Andruh, *New J. Chem.*, 2013, **37**, 2280–2292.
- Y.-N. Guo, X.-H. Chen, S. Xue, and J. Tang, *Inorg. Chem.*, 2012, **51**, 4035–4042.
- H. Ke, S. Zhang, W. Zhu, G. Xie, and S. Chen, *J. Coord. Chem.*, 2015, **68**, 808–822.
- H. Ke, W. Zhu, S. Zhang, G. Xie, and S. Chen, *Polyhedron*, 2015, **87**, 109–116.
- Y.-Z. Zheng, Y. Lan, C. E. Anson, and A. K. Powell, *Inorg. Chem.*, 2008, **47**, 10813–10815.
- B. Gole, K. C. Mondal, and P. S. Mukherjee, *Inorg. Chim. Acta*, 2014, **415**, 151–164.
- K. C. Mondal, G. E. Kostakis, Y. Lan, and A. K. Powell, *Polyhedron*, 2013, **66**, 268–273.
- M. Hasanzadeh, M. Salehi, M. Kubicki, S. M. Shahcheragh, C. Dutkiewicz, M. Pyziak, and A. Khaleghian, *Trans. Met. Chem.*, 2014, **39**, 623–632.
- S. Nayak, H. P. Nayek, S. Dehnen, A. K. Powell, and J. Reedijk, *Dalton Trans.*, 2011, **40**, 2699–2702.
- F. H. Allen, *Acta Crystallogr. Sect. B-Structural Sci.*, 2002, **58**, 380–388.
- P. Bhowmik, N. Aliaga-Alcalde, V. G mez, M. Corbella, and S. Chattopadhyay, *Polyhedron*, 2013, **49**, 269–276.
- R. Ganguly, B. Sreenivasulu, and J. J. Vittal, *Coord. Chem. Rev.*, 2008, **252**, 1027–1050.
- E. Loukopoulos, B. Berkoff, A. Abdul-Sada, G. J. Tizzard, S. J. Coles, A. Escuer, and G. E. Kostakis, *Eur. J. Inorg. Chem.*, 2015, 2646–2649.
- B. Berkoff, K. Griffiths, A. Abdul-Sada, G. J. Tizzard, S. Coles, A. Escuer, and G. E. Kostakis, *Dalton Trans.*, 2015, **44**, 12788–12795.
- K. C. Mondal, A. Sundt, Y. Lan, G. E. Kostakis, O. Waldmann, C. Ungur, L. F. Chibotaru, C. E. Anson, and A. K. Powell, *Angew. Chem. Int. Ed.*, 2012, **51**, 7550–7554.
- I. Nemecek, M. Machata, R. Herchel, R. Bo a, and Z. Tr vni ek, *Dalton Trans.*, 2012, **41**, 14603–14610.
- K. C. Mondal, G. E. Kostakis, Y. Lan, W. Wernsdorfer, C. E. Anson, and A. K. Powell, *Inorg. Chem.*, 2011, **50**, 11604–11611.
- M. Frisch, G. Trucks, and H. Schlegel, *Gaussian Inc., Wallingford, CT*, 2010.
- M. Ernzerhof and G. E. Scuseria, *J. Chem. Phys.*, 1999, **110**, 5029–5036.
- C. Adamo and V. Barone, *Chem. Phys. Lett.*, 1997, **274**, 242–250.
- C. Adamo and V. Barone, *J. Chem. Phys.*, 1999, **110**, 6158.
- C. Adamo, G. E. Scuseria, and V. Barone, *J. Chem. Phys.*, 1999, **111**, 2889.
- C. Adamo and V. Barone, *Theor. Chem. Accounts Theory, Comput. Model. (Theoretica Chim. Acta)*, 2000, **105**, 169–172.
- V. Vetere, C. Adamo, and P. Maldivi, *Chem. Phys. Lett.*, 2000, **32**, 99–105.
- J. Tomasi, B. Mennucci, and R. Cammi, *Chem. Rev.*, 2005, **10**, 2999–3093.
- S. J. Coles and P. A. Gale, *Chem. Sci.*, 2012, **3**, 683–689.

60. O. V Dolomanov, A. J. Blake, N. R. Champness, and M. Schröder, *J. Appl. Crystallogr.*, 2003, **36**, 1283–1284.
61. L. Palatinus and G. Chapuis, *J. Appl. Crystallogr.*, 2007, **40**, 786–790.
62. L. J. Farrugia, *J. Appl. Crystallogr.*, 1999, **32**, 837–838.
63. G. M. Sheldrick, *Acta Crystallogr. Sect. A Found. Adv.*, 2015, **71**, 3–8.
64. G. M. Sheldrick, *Acta Crystallogr. Sect. A*, 2008, **64**, 112–122.
65. A. L. Spek, *J. Appl. Crystallogr.*, 2003, **36**, 7–13.
66. C. F. Macrae, P. R. Edgington, P. McCabe, E. Pidcock, G. P. Shields, R. Taylor, M. Towler, and J. Van De Streek, *J. Appl. Crystallogr.*, 2006, **39**, 453–457.
67. H. H. Thorp, *Inorg. Chem.*, 1992, **31**, 1585–1588.
68. J. L. Atwood and J. W. Steed, in *Supramolecular Chemistry, 2nd Edition*, 2009, p. 402.
69. G. E. Kostakis, V. A. Blatov, and D. M. Proserpio, *Dalton Trans.*, 2012, **41**, 4634–4640.
70. H. Xiang, Y. Lan, L. Jiang, W.-X. Zhang, C. E. Anson, T.-B. Lu, and A. K. Powell, *Inorg. Chem. Commun.*, 2012, **16**, 51–54.
71. Z. Puterová-Tokárová, V. Mrázová, J. Kožíšek, J. Valentová, B. Vranovičová, and R. Boča, *Polyhedron*, 2014, **70**, 52–58.
72. B. Bhattacharya, R. Dey, D. K. Maity, and D. Ghoshal, *CrystEngComm*, 2013, **15**, 9457–9464.
73. K. Griffiths, C. W. D. Gallop, A. Abdul-Sada, A. Vargas, O. Navarro, and G. E. Kostakis, *Chem. Eur. J.*, 2015, **21**, 6358–6361.
74. P. J. Perez, *Alkane C-H Activation by Single-Site Metal Catalysis*, Springer Netherlands, Dordrecht, 2012, vol. 38.
75. M. H. Gubelmann and A. F. Williams, *Struct. Bond.*, 1983, **55**, 2–65.
76. H. A. O. Hill and D. G. Tew, *Comprehensive Coordination Chemistry*, Pergamon Press, Oxford, 1987.
77. C. J. Cramer, W. B. Tolman, K. H. Theopold, and A. L. Rheingold, *Proc. Natl. Acad. Sci. U. S. A.*, 2003, **100**, 3635–3640.
78. J. W. Egan, B. S. Haggerty, A. L. Rheingold, S. C. Sendlinger, and K. H. Theopold, *J. Am. Chem. Soc.*, 1990, **112**, 2445–2446.
79. A. Hess, M. R. Hörz, L. M. Liable-Sands, D. C. Lindner, A. L. Rheingold, and K. H. Theopold, *Angew. Chemie Int. Ed.*, 1999, **38**, 166–168.
80. J. S. Valentine, *Chem. Rev.*, 1973, **73**, 235–245.
81. L. Vaska, *Acc. Chem. Res.*, 1976, **9**, 175–183.
82. A. Wada, S. Ogo, S. Nagatomo, T. Kitagawa, Y. Watanabe, K. Jitsukawa, and H. Masuda, *Inorg. Chem.*, 2002, **41**, 616–618.
83. F. Li, K. K. Meier, M. A. Cranswick, M. Chakrabarti, K. M. Van Heuvelen, E. Münck, and L. Que, *J. Am. Chem. Soc.*, 2011, **133**, 7256–7259.
84. N. F. Chilton, R. P. Anderson, L. D. Turner, A. Soncini, and K. S. Murray, *J. Comput. Chem.*, 2013, **34**, 1164–75.
85. E. V. Alexandrov, A. P. Shevchenko, A. A. Asiri, and V. A. Blatov, *CrystEngComm*, 2015, **17**, 2913–2924.